Aneuploidy triggers autophagy and p53-mediated apoptosis and impairs second lineage segregation in human preimplantation embryos

Marius Regin[1], Yingnan Lei[1], Edouard Couvreu De Deckersberg[1], Yves Guns[2], Pieter Verdyck[3], Greta Verheyen[2], Hilde Van de Velde[2,4], Karen Sermon[1,#], Claudia Spits[1,#]

[1]Research Group Reproduction and Genetics, Faculty of Medicine and Pharmacy, Vrije Universiteit Brussel, Laarbeeklaan 103, 1090 Jette, Brussels, Belgium

[2]Brussels IVF, Universitair Ziekenhuis Brussel, Laarbeeklaan 101, 1090 Jette, Brussels, Belgium

[3]Vrije Universiteit Brussel (VUB), Universitair Ziekenhuis Brussel (UZ Brussel), Clinical Sciences, Research Group Reproduction and Genetics, Centre for Medical Genetics, Brussels, Belgium

[4]Research Group Reproduction and Immunology, Faculty of Medicine and Pharmacy, Vrije Universiteit Brussels, Laarbeeklaan 103, 1090 Jette, Brussels, Belgium

[#]These authors contributed equally to this work.

Corresponding author: Claudia.Spits@vub.be

Abstract

Aneuploidy is present in about 80% of human preimplantation embryos and is thought to largely explain our relatively low fertility. However, the percentage of aneuploid cells decreases progressively during the early cleavages and chromosomally mosaic human embryos have been shown to result in healthy newborns with normal karyotypes. These observations imply a selective loss of aneuploid cells, but the underlying mechanisms are not yet fully understood. Here, we show that, while aneuploid embryos had lower cell numbers in both trophectoderm (TE) and inner-cell-mass (ICM), the effect of aneuploidy was cell-type dependent. Aneuploid TE presented transcriptomic signatures of DNA-damage, p53-signalling and apoptosis. Immunostaining of whole embryos showed that aneuploidy results in increased proteotoxic stress, autophagy, DNA damage-mediated activated p53 and subsequent apoptosis in the TE only. In the ICM, aneuploidy impaired primitive endoderm differentiation. Our findings explain why fully aneuploid embryos fail to further develop

and shed light on the mechanisms by which aneuploid cells are removed from mosaic embryos.

Introduction

Aneuploidy is common in human preimplantation embryos from both natural[1] and medically assisted reproduction[2–4] and is thought to largely explain our relatively low fertility[5,6]. However, chromosomally mosaic embryos can result in healthy newborns with normal karyotypes, implying a selective loss of aneuploid cells during development[7–9]. The underlying mechanisms of this process are not yet fully understood. Here we showed that, while aneuploid embryos had lower cell numbers in both trophectoderm (TE) and inner-cell-mass (ICM), the effect of aneuploidy was cell-type dependent. Aneuploid TE presented transcriptomic signatures of DNA-damage, p53-signalling and apoptosis. Immunostaining of whole embryos showed that aneuploidy results in increased proteotoxic stress, autophagy, DNA damage-mediated activated p53 and subsequent apoptosis in the TE only. In the ICM, aneuploidy impaired primitive endoderm differentiation. Our findings explain why fully aneuploid embryos fail to further develop and by which mechanisms aneuploid cells may be removed from mosaic embryos.

Approximately 80% of human cleavage stage embryos are aneuploid, of which 70% show chromosomal mosaicism, i.e. the presence of at least two cell lineages with different genomic content[10]. The reasons behind this high rate of mitotic errors is still largely unknown but may be a combination of a weak spindle assembly checkpoint (SAC) that is uncoupled of apoptosis until 5 days post fertilization (dpf)[11], in combination with an abundancy of transcripts of anti-apoptotic genes in cleavage-stage embryos[12]. After embryonic genome activation, the rapidly increasing expression of pro-apoptotic genes along with the full functionality of the SAC establishes the control of mitotic errors and the depletion of aneuploid cells from the blastocyst stage on. This is supported by studies showing that the proportion of aneuploid cells within one embryo decreases after 3dpf[9,13] with no apparent preferential allocation of aneuploid cells during first lineage segregation to either TE or ICM[14–16]. After implantation, aneuploid cells become progressively more frequent in the TE lineage as compared to the ICM[16]. This suggest that the extraembryonic tissues are more tolerant

to aneuploidy, in line with the rate of 1-2% of confined placental mosaicism observed in ongoing pregnancies in the general population[17].

The mechanisms behind this selective clearance are thought to be mediated by two well-studied intracellular stress responses[10]. First, aneuploidy results in gene-dosage defects, leading to an unbalanced protein pool and proteotoxic stress. If this remains unresolved by activation of autophagy, CASP8/LC3B/p62 will interact to activate the apoptosis cascade[18–21]. Second, aneuploidy results in replication stress that can lead to DNA-damage, resulting in p53 activation and ultimately to apoptosis[10,22]. In their landmark paper, Bolton *et al*.[23] showed that aneuploid cells are selectively cleared from chimeric mouse embryos generated from control blastomeres mixed with blastomeres treated with the SAC inhibitor reversine. Later work by the same group showed that the apoptosis of these aneuploid cells requires autophagy and *TP53* activation and that euploid cells in the embryo compensate this cell loss by increased proliferation[24]. The authors proposed that the proteotoxic stress observed in these aneuploid chimeric mouse embryos activated the p53 pathway, which in turn activated autophagy and apoptosis. In the study using human gastruloids with reversine-induced aneuploidy, aneuploidy induced apoptosis but without an increase in total p53 expression[9].

These studies have also shown that the apoptotic response to aneuploidy is lineage-specific. In the mouse, aneuploid cells in the ICM are likely eliminated by apoptosis while they are rather tolerated in the TE[23]. Later in development, aneuploid cells are depleted by apoptosis specifically from the mouse epiblast lineage[24]. Similarly, in human gastruloids, aneuploid cells are eliminated by apoptosis from the embryonic germ layers but are tolerated in the TE-like cells[9]. In contrast, mosaic and fully aneuploid human embryos show higher levels of apoptosis in the TE as compared to the ICM[25].

Results and discussion

In the first part of this study, we tested the hypothesis that chromosomally unbalanced cells are cleared during human preimplantation development by apoptosis, mediated by both sustained p62-LC3B accumulation as a marker for autophagy and DNA-damage-mediated p53 activation. Fifty cryopreserved human blastocysts (5 or 6dpf) that had been previously diagnosed by Preimplantation Genetic Testing (PGT) as

either euploid (n=28) or containing non-mosaic aneuploidy (n=22, further referred to as aneuploid, Fig. 1a, Supplementary Table 1) and 11 human cleavage stage embryos that were treated with 0.5 µM reversine from 3dpf to 4dpf and further developed to the blastocyst stage (referred to as reversine-treated embryos, Fig. 1b) underwent a TE biopsy to collect cells for RNA sequencing. Of these, 45 yielded good quality RNA-sequencing results (20 aneuploid, 14 euploid, 11 reversine-treated embryos).

Unsupervised hierarchical clustering and principal component analysis using all expressed genes revealed no clustering of the euploid, aneuploid or reversine-treated embryos in distinct groups (Fig. 1c, Supplementary Fig. 1a). We used InferCNV (https://github.com/broadinstitute/inferCNV/wiki") to bioinformatically infer unbalanced chromosomal copy numbers from gene expression data, based on higher or lower expression of genes located on chromosomes with gains or losses respectively (Fig. 1d, Supplementary Fig. 1b, Supplementary Table 1). We compared the outcomes to the results obtained during PGT and found a match for 43/46 of the full chromosome aneuploidies, while euploidy was correctly predicted in all cases (Supplementary Fig. 1b). These results show that aneuploidy in human blastocysts results in significant abnormal gene dosage effects. The karyotypes of the reversine-treated embryos could not be determined since reversine induces different aneuploidies in each cell, leading to mosaic TE biopsies.

Despite the abnormal gene dosage, and in line with the lack of clear clustering in the PCA, the differential gene expression analysis yielded very few genes with a false discovery rate (FDR-q-value) under 0.05. These findings are similar to those of other studies on the transcriptome of aneuploid human embryos[26,27]. Therefore, we used the differential gene expression with a cutoff value of $|\log_2$ fold change$|>1$ and $-\log_{10}$(p-value) <0.05, and primarily focused on pathway analysis. We found 547 upregulated and 463 downregulated genes in aneuploid versus euploid embryos (Fig. 1e, Supplementary Table 2). Amongst the top upregulated genes was Growth Differentiation Factor 15 (*GDF15*), a gene that has been found to be upregulated in human aneuploid cells[19] including aneuploid human embryos[16]. When comparing reversine-treated versus euploid embryos we observed 539 upregulated and 355 downregulated genes (Fig. 1f, Supplementary Table 3). While only 9.6% of the differentially expressed genes are in common between the aneuploid and reversine-treated embryos (Fig. 1g, h, Supplementary Table 4), pathway analysis revealed

several commonly deregulated pathways. We identified deregulation of the p53 pathway and apoptosis (FDR q-value < 0.05, Fig. 1i, Supplementary Tables 5, 6) and deregulation of cell population proliferation, apoptotic process, regulation of cell death, and cell cycle (Fig. 1j, Supplementary Tables 7, 8). Other pathways of interest related to DNA damage and p53, such as cellular response to DNA damage stimulus and DNA damage response signal transduction by p53 class mediator were specific to the aneuploid group. Cellular senescence signatures in the aneuploid embryos and selective autophagy in the reversine-treated group were also deregulated (Supplementary Tables 9, 10). Ingenuity pathway analysis (IPA) showed that upstream regulators *CDK19* and *AURK* (cell cycle) and *GAS2L3* and *ANLN* (cell growth) were inhibited in the aneuploid group (Fig. 1k, Supplementary Table 11). In line with the GSEA analysis, *p53* was the most activated upstream regulator. Reversine-treated embryos activated *ATM* which is a well-known sensor of DNA-damage that mediates target genes such as *p53*[28] (Fig. 1l, Supplementary Table 12). Canonical pathway analysis by IPA confirmed that p53 signaling, autophagy, cell-cycle pathways and senescence are deregulated in aneuploid embryos (Fig. 1m, Supplementary Table 13). The TE of reversine-treated embryos showed activated senescence, similar to the mouse reversine-treated embryos[23] (Fig. 1n, Supplementary Table 14). Transcription factor analysis identified significant *TP53* expression in both aneuploid groups (Supplementary Tables 15, 16). The connection between aneuploidy, DNA-damage and p53 activation with its downstream effects is also supported by differential expression of several p53 target genes[29] in aneuploid embryos: *MDM2* and *PPM1D* (feedback); *CDKN1A, BTG2, GADD45A* (cell-cycle arrest); *TNFRSF10B* (apoptosis), *DDB2* and *RRM2B* (DNA-repair); *FDXR* (metabolism) and *SESN1* (translation control) (Supplementary Table 2).

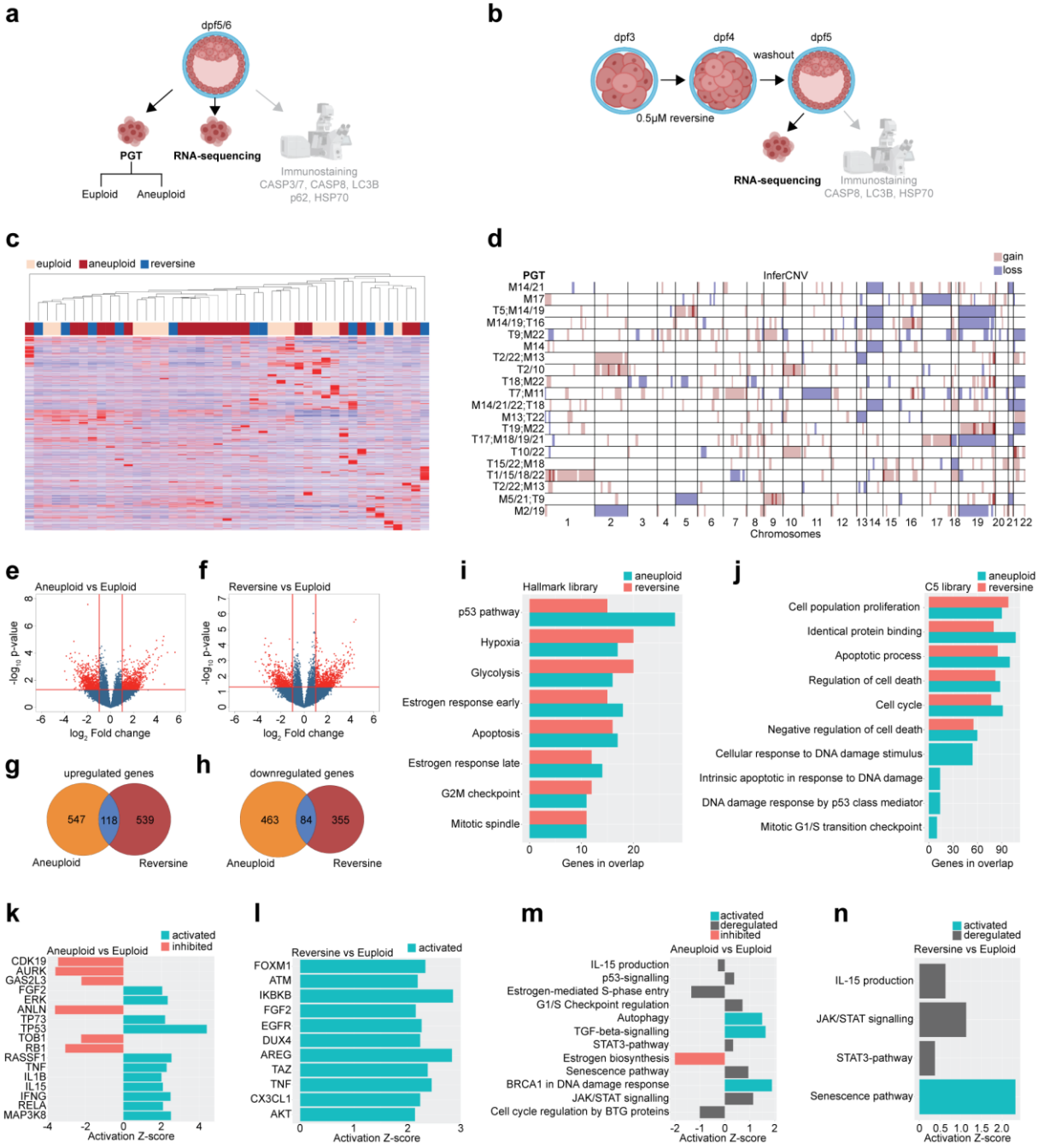

Fig. 1: RNA-sequencing of trophectoderm cells reveals deregulation of DNA damage, p53, cell-cycle, autophagy and apoptosis pathways in chromosomally abnormal human embryos.

a. Human blastocysts 5 or 6 days post-fertilization (dpf) underwent Preimplantation Genetic Testing (PGT) for monogenic diseases and/or aneuploidy screening, followed by cryopreservation. Embryos that were not transferred were donated for research after written informed content. After warming and 2hrs recuperation, euploid and fully aneuploid research embryos underwent a second TE biopsy for RNA-sequencing. The remainder of the embryos was live-stained with either CASP3/7 or CASP8 for 30min and fixed for immunostaining for proteins of interest (see figure 3). **b**. 3dpf human embryos were warmed and treated with 0.5µM reversine for 24hrs then transferred to normal culture medium until 5dpf to undergo TE biopsy for RNA-sequencing. After 2hrs recuperation the embryos were live-stained with CASP8 for 30min and fixed for

immunostaining for proteins of interest (see figure 3). **c**. Unsupervised hierarchical clustering of all coding genes. Color coding: beige = euploid, red = aneuploid and blue = reversine-treated. **d**. Comparison between the diagnosis of aneuploid embryos obtained after PGT (list on the left) and the results obtained after using InferCNV after RNA-sequencing (plot on the right). **e**,**f**. Volcano plots after differential gene expression analysis with a cutoff value of $|\log_2$ fold change$|$ > 1 and $-\log_{10}$(p-value) < 0.05 for aneuploid versus euploid (**e**) and reversine versus euploid (**f**). **g**,**h**. Venn diagrams comparing the upregulated (**g**) and downregulated (**h**) genes in aneuploid versus reversine treated embryos. **i**,**j**. Supervised plot of pathway analysis using the Molecular Signatures Database (FDR < 0.05) based on the list of all differentially expressed genes between aneuploid or reversine versus euploid embryos. Pathways are ranked based on the total number of genes in overlap of both test sets, ranked from sets with the highest number of genes in overlap to sets with the lowest. Outputs of the Hallmark library and C5 ontology gene sets are shown in (**i**) and (**j**), respectively. **k**,**l**. Supervised plots after Ingenuity Pathway Analysis of upstream regulators with an activation z-score ≤ -2 and ≥ 2 and a p-value < 0.05 in the aneuploid (**k**) or reversine (**l**) versus euploid embryos. **m**,**n**. Supervised plots after Ingenuity Pathway Analysis of canonical pathways in aneuploid (**m**) or reversine (**n**) versus euploid embryos. Pathways are ranked by p-value from the most to the least significant, those with a p-value < 0.05 and with an activation z-score ≤ -1.5 and ≥ 1.5 were considered as inhibited or activated, respectively. Significant pathways with an activation z-score between -1.5 and 1.5 were considered as deregulated.

To test if there was a relationship between the level of stress signatures and the size of chromosomal imbalances in embryos[30], we separated the aneuploid group into a low- and a high- imbalanced gene dosage group, based on the total number of coding loci that were affected by the chromosomal abnormalities. The low-dosage group contained the embryos under the 50th percentile when ranking the embryos from the lowest to the highest number of unbalanced loci, the high-dosage group the embryos with 50th percentile or higher (Supplementary Table 17). Hierarchical clustering using the top 500 deregulated genes showed that all high-dosage embryos clustered together and separate from the euploid embryos, while the low-dosage embryos clustered with either group (Fig. 2a). Differential gene expression with $|\log_2$ fold change$|$>1 and $-\log_{10}$(p-value) < 0.05 resulted in 404 upregulated and 340 downregulated genes in low-dosage versus euploid embryos and in 716 upregulated and 627 downregulated genes in high-dosage versus euploid embryos with an overlap of 10% between both groups (Fig. 2b-e, Supplementary Tables 18,19). We identified deregulation of TNFA signaling via NFkB, p53 pathway and apoptosis for both groups (FDR q-value < 0.05, Fig. 2f, Supplementary Tables 20,21). High-dosage embryos additionally showed an unfolded protein response, suggesting that this signature may only be present in the more abnormal embryos. In the high-dosage group more of the genes of the p53 and apoptosis pathways were deregulated, and with higher

significance (Fig. 2g,h, Supplementary Tables 22,23). The gene expression levels in the p53 and apoptosis pathways show a stepwise distribution between the gene dosage groups (Fig. 2i).

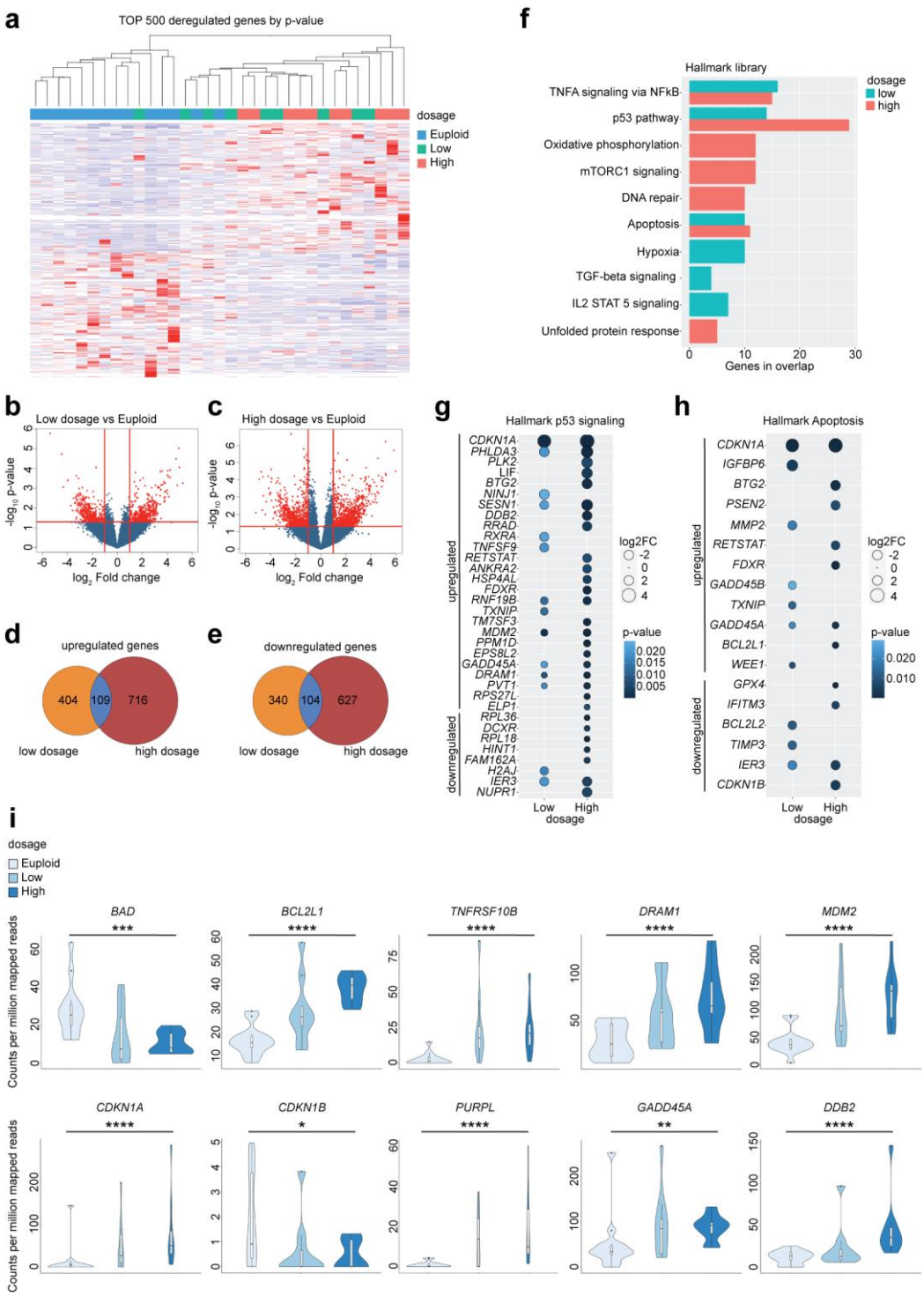

Fig. 2: Human embryos with the highest number of genes with abnormal copy number show stronger p53 pathway and apoptosis response.

a. Supervised hierarchical clustering of the TOP 500 deregulated genes sorted by p-value. Color coding: blue = euploid , green = Low dosage and red = High dosage. **b**,**c**. Volcano plots after differential gene expression analysis with a cutoff value of $|\log_2$ fold change$| > 1$ and $-\log_{10}$(p-value) < 0.05 for low dosage versus euploid embryos (**b**) and high dosage versus euploid embryos (**c**). **d**,**e**, Venn diagrams comparing the upregulated (**d**) and downregulated (**e**) genes in low dosage versus high dosage embryos. **f**. Supervised plot of pathway analysis using the Hallmark library of the Molecular Signatures Database (FDR < 0.05) based on the list of the TOP 500

expressed genes by p-value between low or high dosage versus euploid embryos. Pathways are ranked based on FDR-q-values of both test sets, the most significant deregulated pathway ranked from top to least significant pathway. **g**,**h**. Dot plots of the genes in overlap with the Hallmark p53 pathway (**g**) and Hallmark apoptosis pathway (**h**) of both low and high dosage embryos sorted by $\log_2$ Fold Change from the highest to the lowest. Dots with an increased size and a darker blue represent a higher value of $\log_2$ Fold Change and lower p-value, respectively. **i**, Violin plots with box and whisker plots of the counts per million mapped reads of a supervised set of 10 genes (from Supplementary Table 2) that are part of apoptosis (*BAD, BCL2L1, TNFRSF10B*), p53 pathway (*DRAM1, MDM2, CDKN1A/B, PURPL*), growth arrest (*GADD45A*), and DNA-damage (*DDB2*). *p = 0.027, **p = 0.010, ***p = 0.004, ****p < 0.001 using the Jonkheere-Terpstra test. Box and whisker plots show median and minimum to maximum values.

To confirm our transcriptomic findings, we immunostained the remainder of the embryos after TE biopsy. Thirty-seven (18 euploid, 19 aneuploid) of the 50 PGT embryos and 8 reversine-treated embryos were successfully stained for markers of apoptosis, proteotoxic stress and autophagy (Fig. 3a,b). Aneuploid embryos showed increased intensity levels of active CASP3/7 (13 euploid, 8 aneuploid) and CASP8 (6 euploid, 9 aneuploid, 8 reversine-treated) (Fig. 3c-f). Both aneuploid and reversine-treated embryos had lower cell numbers than euploid embryos (Fig. 3g). We investigated whether proteotoxic stress and autophagy[18,19,21–24] were also present in aneuploid human embryos. The number of puncta per cell of autophagy markers LC3B (19 euploid, 22 aneuploid, 8 reversine-treated) and p62 (6 euploid, 9 aneuploid) and the intensity levels of proteotoxic stress marker HSP70 (13 euploid, 8 aneuploid, 8 reversine-treated) were significantly increased in both aneuploid and reversine-treated embryos (Fig. 3h-k). The gene expression profiles suggest that the accumulation of autophagic proteins in aneuploid embryos is caused by increased autophagic flux due to differential expression of the *p53* target gene DNA Damage Regulated Autophagy Modulator-1 (*DRAM1*), rather than by inhibition of autophagy (Supplementary Table 2). This protein is located in the lysosomal membrane and in cancer cells it increases autophagic flux and apoptosis after stress-induced p53 activation[31,32].

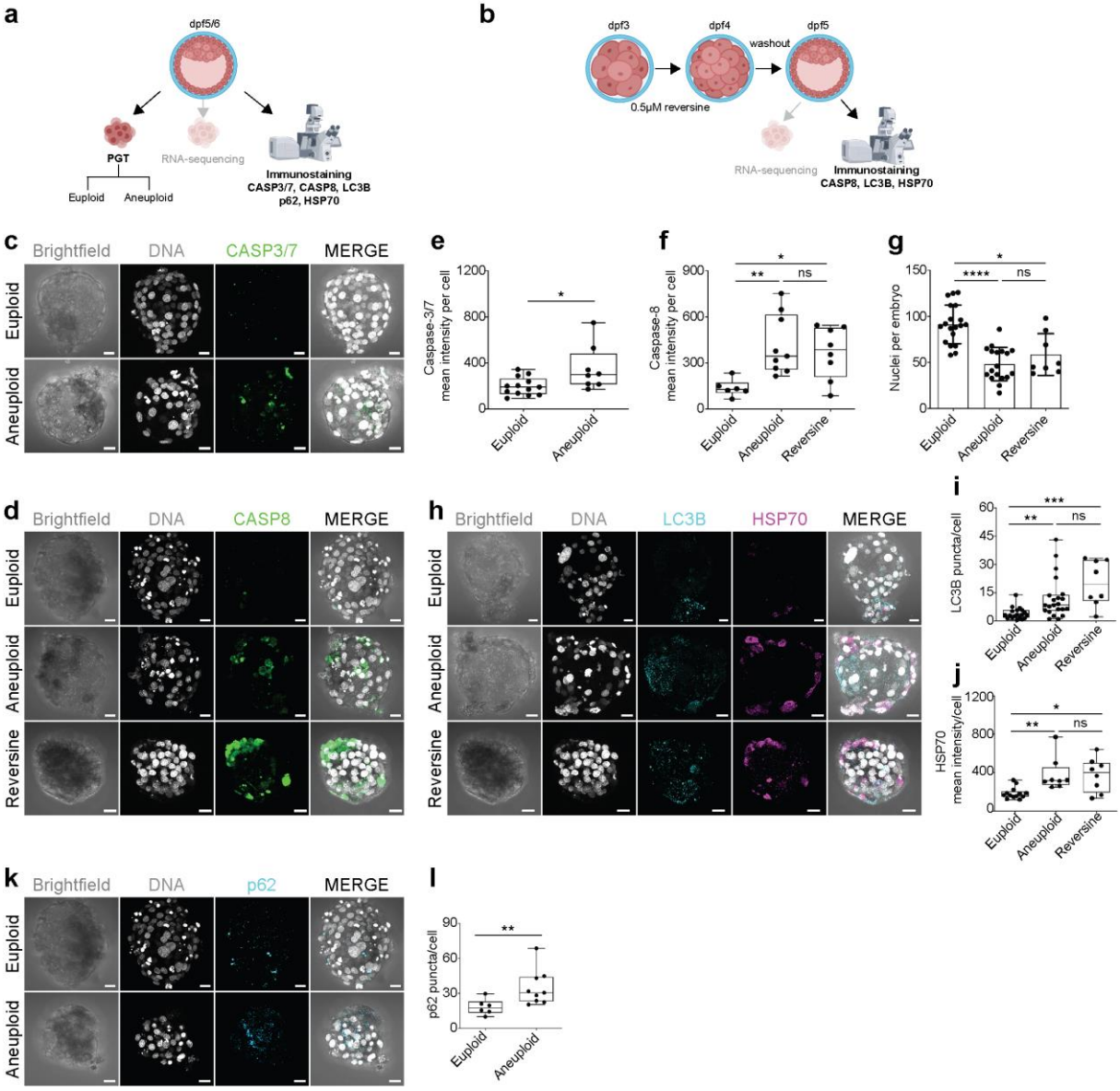

Fig. 3: Immunostaining reveals increased apoptosis, autophagy, proteotoxic stress and DNA-damage in chromosomally abnormal human embryos.
a,**b**. Same experimental set-up as described in **Fig. 1 a**,**b**, but focused on immunostaining analysis. **c**, Orthogonal projections after immunostaining of euploid and aneuploid embryos for DNA (white) and CASP3/7 (green). **d**, Orthogonal projections after immunostaining of euploid, aneuploid and reversine-treated embryos for DNA (white) and CASP8 (green). **e**, CASP3/7 mean intensity per cell. Euploid n=13, Aneuploid n=8 embryos. Mann-Whitney test, *p = 0.0199. **f**, CASP8 mean intensity per cell. Euploid n=6, Aneuploid n=9, Reversine-treated n=8 embryos. Kruskal-Wallis test, *p = 0.0394, **p = 0.0085. **g**, Number of nuclei per embryo. Euploid n=19, Aneuploid n=18, Reversine-treated n=8 embryos. Kruskal-Wallis test, ****p < 0.0001, *p = 0.0305. **h**, Orthogonal projections after immunostaining of euploid, aneuploid and reversine-treated embryos for DNA (white), LC3B (turquoise) and HSP70 (magenta). **i**, LC3B puncta per cell. Euploid n=19, Aneuploid n=22 embryos, Reversine-treated n=8 embryos. Kruskal-Wallis test, *p = 0.0189, **p = 0.0074. **j**, HSP70 mean intensity per cell. Euploid n=13, Aneuploid n=8, Reversine-treated n=8 embryos. Kruskal-Wallis test, **p = 0.0077, ***p = 0.0008. **k**, Orthogonal projections after immunostaining of

euploid, aneuploid for DNA (white) and p62 (turquoise). **l**, p62 puncta per cell. Euploid n=6, Aneuploid n=9 embryos. Mann-Whitney test, **p = 0.0076.
Brightfield pictures were obtained during confocal imaging. All scale bars are 20 µm. Box and whisker plots show median and whiskers show minimum to maximum values. Bar plots show mean ± s.d. For all plots each dot represents a single embryo and ns = not significant.

We further investigated if these effects are cell-type specific and how they affect the first lineage segregation to TE and ICM, and the second to epiblast (EPI) and primitive endoderm (PrE), as suggested by the mouse studies[23,24] and the work on human gastruloids[9]

We co-stained another batch of embryos for OCT4 (10 euploid, 14 aneuploid, ICM) and CASP3/7 (10 euploid, 14 aneuploid), LC3B (4 euploid, 5 aneuploid) or Serine 15 p53 (3 euploid, 5 aneuploid) (Fig. 4a, Supplementary Table 24). The latter marker was chosen to demonstrate that the transcriptomic signature of p53 signaling is caused by DNA-damage-induced phosphorylation of Serine-15 on p53[33]. All embryos were then re-stained with GATA4 (PrE) and imaged together with OCT4 to investigate the impact of aneuploidies on the second lineage segregation. Aneuploid embryos showed a higher percentage of cells with activated p53 (Fig. 4b,c), although these differences did not reach significance when considering the ICM or TE separately (Supplementary Fig. 1c-e), and showed decreased cell numbers in both the ICM and TE (Fig. 4d-g). The observed increased percentage of nuclear CASP3/7 positive cells in the TE of aneuploid embryos (Fig. 4h,i) and increased CASP3/7 mean intensity per cell in whole aneuploid embryos (Fig. 4j) may explain how apoptosis caused this decrease in cell numbers. However, no ICM cells of either group showed full nuclear CASP3/7 signal. We also found CASP3/7-positive micronuclei which were significantly increased in number in aneuploid embryos (Supplementary Fig. 1f,g). This is similar to findings in a non-human primate model showing that abnormal chromosomes can be encapsulated in micronuclei, which can subsequently be selectively eliminated from the embryo[34]. In human cleavage stage embryos these micronuclei have been shown to contain genetic material that originates from chromosome breakages due to replication fork stalling and DNA-damage during the first cell-cycle[35].

The decreased cell numbers in the ICM in absence of apoptosis could be explained by two other known effects of p53 activation. First, p53-mediated decreased proliferation

could result in lower cell numbers. Secondly, *TP53* activation may downregulate *OCT4* and *NANOG*, as seen in mouse embryonic stem cells[36], leading to loss of pluripotency and driving the cells to differentiation and out of the ICM.

We therefore investigated the consequences of aneuploidies on the second lineage segregation, by determining the cell-type composition of the ICM by using GATA4 as PrE marker and OCT4 as an ICM marker. We found that while all euploid embryos contained GATA4-positive cells, 7/14 aneuploid embryos had an ICM with no GATA4-positive cells (Fig. 4k,l). Further, in those aneuploid embryos with a GATA4-positive PrE, we observed a significantly lower PrE/EPI ratio (Fig. 4m). This suggests that either aneuploid embryos fail to form PrE or that this lineage is more sensitive to aneuploidy-mediated apoptosis, indicating that euploidy is important for the correct onset and/or maintenance of the second lineage differentiation.

The higher levels of autophagy in TE as compared to the ICM suggest that pluripotent cells are less sensitive to aneuploidies, as described in the human gastruloid model[9]. Aneuploid embryos displayed significantly increased levels of autophagy mainly attributable to the TE (Fig. 4n-q), while their ICMs showed a small increase in autophagy which does not reach significance (Fig. 4q). Remarkably, the aneuploid embryos could be separated in two groups: a first group with low levels of autophagy lacking GATA4-positive cells in 2 out of 3 embryos (Fig. 4n, left and right panels, 2nd row) and a high-level autophagy group in which both embryos contained GATA4-positive cells (Fig. 4n, left and right panels 3rd row). Although based on a few samples, this data suggests that an ICM in a transcriptionally earlier state of pluripotency, i.e. GATA4-negative, might be less sensitive to the consequences of aneuploidy, i.e. show less autophagy. We also found that aneuploid embryos split into two groups in terms of number of ICM cells: one with similar number of cells as the euploid ICM which we suggest have not initiated PrE differentiation, and one with very low number of cells or no ICM, which supports our suggestion that GATA4-positive cells are more sensitive to apoptosis (Fig. 4f). Lastly, we separated the aneuploid embryos into a low- and a high-dosage group as done for the gene-expression analysis (Supplementary Table 25). Trend analysis showed that the higher the number of imbalanced loci, the lower the cell numbers in the TE and PrE but not in the ICM (Fig. 4r)[9,16].

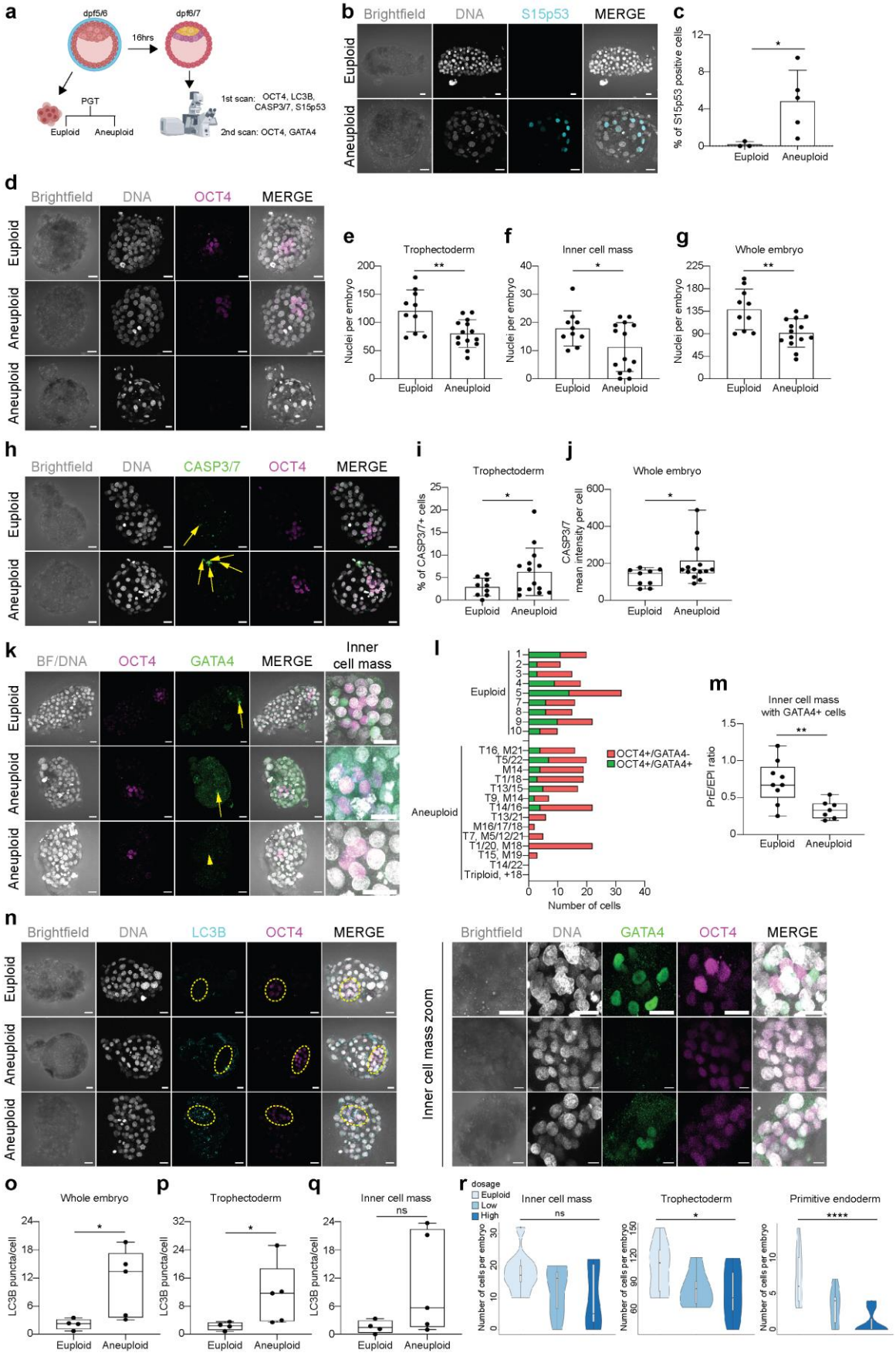
a
dpf5/6
16hrs
dpf6/7
PGT
Euploid
Aneuploid
1st scan: OCT4, LC3B, CASP3/7, S15p53
2nd scan: OCT4, GATA4
b
Brightfield
DNA
S15p53
MERGE
Euploid
Aneuploid
c
% of S15p53 positive cells
Euploid
Aneuploid
d
Brightfield
DNA
OCT4
MERGE
Euploid
Aneuploid
Aneuploid
e
Trophectoderm
Nuclei per embryo
f
Inner cell mass
g
Whole embryo
h
Brightfield
DNA
CASP3/7
OCT4
MERGE
i
Trophectoderm
% of CASP3/7+ cells
j
Whole embryo
CASP3/7 mean intensity per cell
k
BF/DNA
OCT4
GATA4
MERGE
Inner cell mass
l
Euploid
Aneuploid
OCT4+/GATA4-
OCT4+/GATA4+
Number of cells
m
Inner cell mass with GATA4+ cells
PrE/EPI ratio
n
Brightfield
DNA
LC3B
OCT4
MERGE
Inner cell mass zoom
GATA4
o
Whole embryo
LC3B puncta/cell
p
Trophectoderm
q
Inner cell mass
ns
r
dosage
Euploid
Low
High
Inner cell mass
Trophectoderm
Primitive endoderm
Number of cells per embryo

Fig. 4: Aneuploid human embryos show less cells in trophectoderm and inner cell mass and impaired primitive endoderm differentiation

a, 5 or 6dpf post-PGT-A euploid and fully aneuploid human blastocysts were warmed and kept for 16hrs in culture to allow for second lineage segregation. The blastocysts were live-stained with CASP3/7 for 30min and fixed for immunostaining proteins of interest. In a first scan we analyzed OCT4 (ICM), CASP3/7 (apoptosis), LC3B (autophagy) and S15p53 (DNA damage) in both lineages. Embryos were then re-stained with GATA4 as a marker for PrE. **b,** Orthogonal projections after immunostaining of euploid, aneuploid for DNA (white) and Serine (S) 15 p53 (turquoise). **c**, Percentage (%) of Serine 15 p53 positive cells per embryo. Euploid n = 3, Aneuploid n = 5. Mann-Whitney test, *p = 0.0357. **d**, Orthogonal projections after immunostaining of euploid and aneuploid embryos for DNA (white) and OCT4 (magenta). The first aneuploid panel shows a similar number of ICM cells compared to the euploid embryo. The second aneuploid panel shows an embryo without an ICM. **e,f**,**g**, Differences in number of nuclei per embryo between euploid and aneuploid embryos in the trophectoderm (**e**) **p = 0.0092 , inner cell mass *p = 0.0412 (**f**) and whole embryo **p = 0.0067 (**g**). Euploid n = 10, Aneuploid n = 14. Student's t-test with Welch's correction**.** **h**, Orthogonal projections after immunostaining of euploid and aneuploid embryos for DNA (white), CASP3/7 (green) and OCT4 (magenta). **i**, Percentage (%) of CASP3/7 positive (+) cells in the trophectoderm lineage. Euploid n = 9, Aneuploid n = 14. Student's t-test with Welch's correction, *p = 0.0453. **j**, CASP3/7 mean intensity per cell of whole embryos. Euploid n = 9, Aneuploid n = 14. Student's t-test with Welch's correction, *p = 0.0332. **k**, Orthogonal projections after immunostaining of euploid and aneuploid embryos for DNA (white), OCT4 (magenta) and GATA4 (green). The first aneuploid panel shows an embryo with presence of a GATA4 positive cell. The second aneuploid panel shows an embryo that did not contain GATA4 positive cells. **l**, Differences in the number of cells per embryo that were OCT4 positive and either GATA4 negative (red) or positive (green) between euploid and aneuploid embryos. In case GATA4-positive cells (PrE) were present we considered the GATA4-negative cells to be epiblast (EPI). All euploid embryos contained GATA4-positive cells, 7/14 aneuploid embryos had an ICM completely lacking GATA4-positive cells (Fisher-exact test, p = 0.0188). **m**, Differences in the PrE/EPI ratio between euploid and aneuploid embryos that had an ICM containing GATA4-positive cells. Euploid n = 9, Aneuploid n = 7. Note here that one euploid embryo (#6, **l**) was lost during re-staining for GATA4. Mann-Whitney test, **p = 0.0089. **n**, Orthogonal projections after immunostaining of euploid and aneuploid embryos for DNA (white), LC3B (turquoise) and OCT4 (magenta). Yellow circle indicates the ICM. The first aneuploid panel shows an ICM with low levels of autophagy and, after re-staining for GATA4, without PrE (right panel, ICM zoom). The second aneuploid panel shows an embryo with high levels of autophagy in the ICM that contains PrE cells (right panel, ICM zoom). **o,p,q.** Differences in LC3B puncta per cell between euploid and aneuploid embryos in the whole embryo,*p = 0.0317 (**o**), TE,*p = 0.0317 (**p**) and ICM (**q**). Euploid n = 4, Aneuploid n = 5. Mann-Whitney test. **r**, Violin plots with box plots of ICM cells per embryo (left, ns), TE cells per embryo (center, *p = 0.043) and PrE cells per embryo (right, ****p < 0.001, Jonkheere-Terpstra test) depending on gene dosage. Euploid (light blue), Low dosage (middle blue) and High dosage (darkest blue).

Yellow arrows indicate presence of the signal and yellow arrow heads indicate absence of signal. Brightfield pictures were obtained during confocal imaging. All scale bars are 20 µm. Box and whisker plots show median and minimum to maximum values. Bar plots show mean ± s.d. For all plots each dot represents a single embryo; ns = not significant.

In conclusion, our study shows by which molecular cascades aneuploid cells are removed from the human preimplantation embryo. We identified two different stress responses, proteotoxic stress and DNA-damage mediated p53 activation, that can both lead to autophagy activation and downstream cell-cycle arrest, senescence and, ultimately, apoptosis. Overall, our results are in line with previously published RNA-sequencing results on aneuploid human embryonic cells that present transcriptional signatures consistent with DNA damage[37,38], alteration of cell proliferation[16,27] and the cell cycle[37,38], and deregulation of autophagy[38,39], p53 signaling[38] and apoptosis[26,27,38,39]. Naturally acquired and induced aneuploidies only share a few differentially expressed genes but show overall equal signatures after pathway analysis, suggesting that reversine-based models of aneuploidy do not fully mimic endogenous aneuploidy. Aneuploidy impaired TE/ICM formation and PrE differentiation, which might explain aneuploidy-related developmental arrest. Whether this is also driven by p53 activation remains to be confirmed. We propose that aneuploid human embryonic cells in the ICM become more sensitive from the second lineage segregation onwards and hypothesize that this effect may even become stronger and more specific to the embryonic lineage after onset of gastrulation[9]. This is different to the mouse model, which can deplete aneuploid cells specifically from the embryonic lineage before implantation[23,24].

Taken together, our results provide insight into the mechanisms by which mosaic embryos are overcoming aneuploidy and are able to further develop into healthy newborns, as widely observed in clinical practice of reproductive medicine, and on how aneuploidy can result in early pregnancy loss. Further research will shed light on the interactions between the p53 pathway and differentiation during early development, for which the most novel models of post-implantation[40–42] human development will prove to be of incalculable value.

Methods

Human pre-implantation embryos. All experiments have been approved by the local Commission of Medical Ethics of the UZ Brussels (B.U.N. 143201628722) and the Federal Committee for Medical and Scientific Research on Human Embryos *in vitro* (AdV069 and AdV091). Patients from Brussels IVF (University Hospital Brussels) donated their embryos for research after written informed consent. We warmed vitrified human blastocysts after PGT or at 3dpf using the Vitrification Thaw Kit (Vit Kit-Thaw; Irvine Scientific, USA) following manufacturer's instructions. Post PGT-embryos were left to recover for 2h in 25 µL droplets of Origio Sequential Blast™ medium (Origio) at 37°C with 5% O_2, 6% CO_2 and 89% N_2, after which they underwent a second TE biopsy (Fig. 1a). For the reversine experiment, we cultured the 3dpf embryos for 24h in the same medium supplemented with 0.5 µM reversine (Stem Cell Technologies) and after wash-out we let them develop until 5dpf and subsequently took a biopsy (Fig. 1b). The PGT embryos used for the second experiment series (Fig. 4a) were cultured for 16h after warming. Prior to fixation we live-stained all the embryos with either Caspase-3/7 or Caspase-8 (Supplementary Table 26) for 30 min and subsequently removed the zona pellucida using Acidic Tyrode's Solution (Sigma-Aldrich) for 30 sec – 2 min and subsequently washed in PBS/2%BSA.

Biopsy procedure. The zona pellucida was opened (15-25µm) on 4dpf using a Saturn Laser (Cooper Surgical). For PGT cycles**,** fully expanded good quality embryos were biopsied 5dpf. Early blastocysts were evaluated again on day 6. Briefly, embryos were transferred to HEPES buffered medium and biopsied on a Nikon inversed microscope equipped with a Saturn Laser. The herniated TE cells were then aspirated and cut using manual laser shoots. In case of sticking cells this was supported by mechanical cutting. After successful tubing, the blastocysts were vitrified using CBS-VIT High-Security straws (CryoBioSystem, L'Aigle, France) with dimethylsulphoxide-ethylene glycol-sucrose as the cryoprotectants (Irvine Scientific Freeze Kit, Newtownmountkennedy, County Wicklow, Ireland)[43]. The TE biopsy for RNA-sequencing (Fig. 1a,b) was performed with the same procedure, cells were biopsied form the same opening in the zona pellucida.

PGT. During PGT we analyzed a TE sample with multiple cells for each embryo. Next Generation Sequencing: The chromosomal analysis has been performed by WGA

(Sureplex, Illumina) followed by library preparation (KAPA HyperPlus, Roche), sequencing on a NovaSeq (Illumina) and an *in-house* developed interpretation pipeline. The analysis has an effective resolution of 5 Mb.

SNP-array: We relied on whole genome amplification (MDA, Repli-G) followed by genome wide SNP array using Karyomapping (Vitrolife) with Bluefuse software (Vitrolife). In addition, SNP array data were analyzed with an *in-house* developed interpretation pipeline for aneuploidy detection.

RNA-sequencing. Multiple (5-10) TE cells were used as input to generate full length cDNA with the SMART-Seq™ v4 Ultra™ Low Input RNA Kit (Clontech Laboratories, Inc.) according to the manufacturer's instructions. The quality of cDNA was checked using the AATI Fragment Analyzer (Advances Analytical). Library preparation was performed using the KAPA HyperPlus Library Preparation Kit (KAPA Biosystems) according to the manufacturer's instructions. During cDNA synthesis and library preparation we used 17 and 11 PCR cycles, respectively. Sequencing was performed on a NovaSeq 6000 (Illumina) with 25 million reads per sample.

Bioinformatics analysis. Reads were trimmed using cutadapt version 1.11 to remove the "QuantSEQ FWD" adaptor sequence. We checked the quality of the reads using the FastQC algorithm[44]. Count tables were generated using STAR[45] (version 2.5.3) through mapping against the Genome Reference Consortium Human Build 38 patch release 10 (GRCh38.p10) combined with a general transfer format (GTF) file, both downloaded from the Ensembl database. The RNA-sequencing by Expectation Maximization (RSEM)[46] software (version 1.3.0) was used to produce the count tables.

Differential gene expression analysis was performed using R-studio (Version 1.1.456) with the edgeR[47] and limma[48] packages. We included genes with a count per million greater than 1 in at least two samples. The trimmed mean of M values[49] algorithm was used for normalization. The normalized counts were then transformed in a $\log_2$ fold-change ($\log_2$FC) table with their associated statistics. In each comparison, genes with a $|\log_2 FC| > 1$ and an p-value < 0.05 were considered as significantly differentially expressed.

Gene set enrichment analysis (GSEA) was performed using the 'investigate gene sets' function on the website of the Molecular Signature Database (http://www.gsea-

msigdb.org/gsea/msigdb/annotate.jsp). We used all differentially expressed genes (Supplementary Tables 2, 3) as input and investigated Hallmark, C2 and C5 gene sets with FDR-q values < 0.05. For the analysis of gene dosage effects, we could only use the TOP500 differentially expressed genes by p-value since the Molecular Signature Database changed the cut-off during the period of our data analysis (raw data, Supplementary Tables 22,23). In the figures 1f and g we used a supervised approach and sorted the significantly deregulated gene sets by the total amount of genes in overlap. Figure 2f was also supervised but the gene sets were sorted by FDR-q value.

Ingenuity Pathway analysis (IPA, Qiagen Inc.) was used to investigate activated, deregulated and inhibited upstream regulators and canonical pathways. As for the GSEA we used all differentially expressed genes of our two test sets with their respective $\log_2$FC and p-value. For the upstream regulators IPA computes z-scores with associated p-values that are considered significant when $p < 0.05$. If significant, a z-score > 2 means activated, a z-score < 2 means inhibited and in between means deregulated. For the canonical pathways IPA computes z-scores with associated p-values that are considered significant when $p < 0.05$. If significant, we considered a z-score > 1.5 as activated, a z-score < 1.5 as inhibited and in between as deregulated. We generated all figures in a supervised approach.

Transcription factor analysis of all differentially expressed genes was performed using Enrichr (https://maayanlab.cloud/Enrichr/). We selected the outputs from ChEA 2016 and ENCODE ChEA consensus and considered those transcription factors as significant with a p-value < 0.05.

The copy number variation (CNV) analysis was inferred from our RNA-sequencing data set using *inferCNV* R package (version 1.7.1) (Inferring copy number alterations from tumor single cell RNA-Seq data (https://github.com/broadinstitute/inferCNV/wiki"). Our count table was used as input and compared to the reference set which in our case was the expression data of the euploid embryos. The analysis followed the standard workflow in inferCNV with the following parameters: “denoise” mode, value of 1 was used for the “cutoff”, prediction of CNV states using default Hidden Markov Models (HMM) method, “cluster_by_groups” was set to TRUE, and other values were set by default.

All figures were generated using R-studio (Version 1.1.456).

Gene dosage analysis. We calculated the total number of loci with imbalanced gene expression based on the genetic abnormalities identified during the PGT. For this, we used the number of coding loci per chromosomal region as listed in the ENSMBL database (ensemble.org) and included both gains and losses, either mosaic or homogeneously present, and both full chromosomal aneuploidy as well as segmental abnormalities. The embryos were ranked based on the total number of imbalanced loci and separated into a low- and a high-imbalanced gene dosage group. The low-dosage group contained the embryos with the lowest 50th percentile in number of unbalanced loci, the high-dosage group the embryos with 50th percentile or higher (Supplementary Table 17, 25).

Immunocytochemistry. Embryos were fixed using 4% paraformaldehyde (Sigma-Aldrich) for 10 min, washed three times in PBS/2%BSA for 5 min and then permeabilized using 0.1% Triton X-100 (Sigma-Aldrich) for 20 min followed by another washing cycle. We used 10% FBS supplemented with 2% BSA for 1h to block non-specific protein binding. The embryos were then incubated overnight with primary antibodies (Supplementary Table 26) diluted in blocking buffer at 4°C. The next day, they underwent another washing cycle using PBS/2%BSA and were then incubated with secondary antibodies (1:200, Supplementary Table 26) for 1h at room temperature. After washing, nuclei were stained using Hoechst 33342 (5µg/mL, Life Technologies) diluted in PBS/2%BSA for 15 min. For imaging we mounted the embryos on poly-L-lysine coated glass slides (Sigma-Aldrich) in 3µL of PBS. To avoid flattening of the embryos we used Secure-Seal™ Spacers (9mm diameter, 0.12mm deep, Thermofisher) before putting the coverslips in place. For the experiments that required re-staining (Fig. 4a) we imaged the embryos in 3µL PBS/2%BSA in 18 well µ-Slides (Ibidi) and subsequently recuperated them. After recuperation we photobleached the embryos stained for CASP3/7 by using maximum laser power of the 488 nm channel and maximum size of the pinhole for 10 min. The embryos were then re-stained using rat-anti-GATA4 primary antibody and the matching Alexa Fluor 488 secondary antibody (Supplementary Table 26) (to replace the CASP3/7 staining).

Imaging and image analysis. Confocal imaging was performed using the LSM800 (Zeiss). Z-stacks were taken with a LD C-Apochromat 40x/1.1 NA water immersion

objective in optical sections of 1µm. Nuclei were counted using Arivis Vision 4D (3.4.0). All other measurements were performed using the Zen 2 (blue edition) software based on the optical sections and/or orthogonal projections.

Statistics. The type of statistical test and p-values are mentioned in the figure legends. For experiments that contained groups with small sample sizes we used non-parametric tests (Mann-Whitney or Kruskal-Wallis test). Fisher-exact test was used to determine the dependency of the ploidy status on the presence or absence of primitive endoderm. Otherwise we used Student's t-test with Welch's correction when we assumed normal distribution and unequal standard deviations. We used GraphPad Prism 9.0.0 or R-studio for statistical testing. The trend analysis regarding gene dosage effects was performed with SPSS using the Jonkheere-Terpstra test.

References

1. Munné, S. *et al.* First PGT-A using human in vivo blastocysts recovered by uterine lavage: Comparison with matched IVF embryo controls. *Human Reproduction* **35**, 70–80 (2020).
2. Mertzanidou, A. *et al.* Microarray analysis reveals abnormal chromosomal complements in over 70% of 14 normally developing human embryos. *Human Reproduction* **28**, 256–264 (2013).
3. Mertzanidou, A., Spits, C., Nguyen, H. T., Van de Velde, H. & Sermon, K. Evolution of aneuploidy up to Day 4 of human preimplantation development. *Human Reproduction* **28**, 1716–1724 (2013).
4. Vanneste, E. *et al.* Chromosome instability is common in human cleavage-stage embryos. *Nat Med* **15**, 577–583 (2009).
5. DELHANTY, J. D. A. Preimplantation genetics: an explanation for poor human fertility? *Ann Hum Genet* **65**, 331–338 (2001).
6. Macklon, N. S., Geraedts, J. P. M. & Fauser, B. C. J. M. Conception to ongoing pregnancy: The ‘black box’ of early pregnancy loss. *Hum Reprod Update* **8**, 333–343 (2002).
7. Greco, E., Minasi, M. G. & Fiorentino, F. Healthy Babies after Intrauterine Transfer of Mosaic Aneuploid Blastocysts. *New England Journal of Medicine* **373**, 2089–2090 (2015).
8. Viotti, M. *et al.* Using outcome data from one thousand mosaic embryo transfers to formulate an embryo ranking system for clinical use. *Fertil Steril* **115**, 1212–1224 (2021).
9. Yang, M. *et al.* Depletion of aneuploid cells in human embryos and gastruloids. *Nat Cell Biol* **23**, 314–321 (2021).
10. Regin, M., Spits, C. & Sermon, K. On the origins and fate of chromosomal abnormalities in human preimplantation embryos: an unsolved riddle. *Mol Hum Reprod* (2022) doi:10.1093/molehr/gaac011.
11. Jacobs, K., van de Velde, H., de Paepe, C., Sermon, K. & Spits, C. Mitotic spindle disruption in human preimplantation embryos activates the spindle assembly checkpoint but not apoptosis until Day 5 of development. *MHR: Basic science of reproductive medicine* **23**, 321–329 (2017).

12. Yan, L. *et al.* Single-cell RNA-Seq profiling of human preimplantation embryos and embryonic stem cells. *Nat Struct Mol Biol* **20**, 1131–1139 (2013).
13. van Echten-Arends, J. *et al.* Chromosomal mosaicism in human preimplantation embryos: a systematic review. *Hum Reprod Update* **17**, 620–627 (2011).
14. Capalbo, A. *et al.* FISH reanalysis of inner cell mass and trophectoderm samples of previously array-CGH screened blastocysts shows high accuracy of diagnosis and no major diagnostic impact of mosaicism at the blastocyst stage. *Human Reproduction* **28**, 2298–2307 (2013).
15. Popovic, M. *et al.* Chromosomal mosaicism in human blastocysts: The ultimate challenge of preimplantation genetic testing? *Human Reproduction* **33**, 1342–1354 (2018).
16. Starosti, M. R., Sosin, O. A. & McCo, R. C. Single-cell analysis of human embryos reveals diverse patterns of aneuploidy and mosaicism. *Genome Res* **30**, 814–826 (2020).
17. Kalousek, D. K. & Vekemans, M. Confined placental mosaicism. *Journal of Medical Genetics* vol. 33 529–533 Preprint at https://doi.org/10.1136/jmg.33.7.529 (1996).
18. Stingele, S. *et al.* Global analysis of genome, transcriptome and proteome reveals the response to aneuploidy in human cells. *Mol Syst Biol* **8**, 608 (2012).
19. Dürrbaum, M. *et al.* Unique features of the transcriptional response to model aneuploidy in human cells. *BMC Genomics* **15**, 139 (2014).
20. Pan, J.-A., Ullman, E., Dou, Z. & Zong, W.-X. Inhibition of protein degradation induces apoptosis through a microtubule-associated protein 1 light chain 3-mediated activation of caspase-8 at intracellular membranes. *Mol Cell Biol* **31**, 3158–70 (2011).
21. Ohashi, A. *et al.* Aneuploidy generates proteotoxic stress and DNA damage concurrently with p53-mediated post-mitotic apoptosis in SAC-impaired cells. *Nat Commun* **6**, 1–16 (2015).
22. Zhu, J., Tsai, H. J., Gordon, M. R. & Li, R. Cellular Stress Associated with Aneuploidy. *Developmental Cell* vol. 44 420–431 Preprint at https://doi.org/10.1016/j.devcel.2018.02.002 (2018).

23. Bolton, H. *et al.* Mouse model of chromosome mosaicism reveals lineage-specific depletion of aneuploid cells and normal developmental potential. *Nat Commun* **7**, 1–12 (2016).
24. Singla, S., Iwamoto-Stohl, L. K., Zhu, M. & Zernicka-Goetz, M. Autophagy-mediated apoptosis eliminates aneuploid cells in a mouse model of chromosome mosaicism. *Nat Commun* **11**, 1–15 (2020).
25. Victor, A. R. *et al.* One hundred mosaic embryos transferred prospectively in a single clinic: exploring when and why they result in healthy pregnancies. *Fertil Steril* **111**, 280–293 (2019).
26. Groff, A. F. *et al.* RNA-seq as a tool for evaluating human embryo competence. *Genome Res* **29**, 1705–1718 (2019).
27. Maxwell, S. M. *et al.* Investigation of Global Gene Expression of Human Blastocysts Diagnosed as Mosaic using Next-generation Sequencing. *Reproductive Sciences* 1–11 (2022) doi:10.1007/s43032-022-00899-x.
28. Banin, S. *et al.* Enhanced phosphorylation of p53 by ATM in response to DNA damage. *Science* **281**, 1674–1677 (1998).
29. Jaiswal, S. K., Raj, S. & DePamphilis, M. L. Developmental Acquisition of p53 Functions. *Genes (Basel)* **12**, 1675 (2021).
30. Dürrbaum, M. & Storchová, Z. Effects of aneuploidy on gene expression: implications for cancer. *FEBS J* **283**, 791–802 (2016).
31. Crighton, D. *et al.* DRAM, a p53-Induced Modulator of Autophagy, Is Critical for Apoptosis. *Cell* **126**, 121–134 (2006).
32. Guan, J. J. *et al.* DRAM1 regulates apoptosis through increasing protein levels and lysosomal localization of BAX. *Cell Death Dis* **6**, e1624–e1624 (2015).
33. Loughery, J., Cox, M., Smith, L. M. & Meek, D. W. Critical role for p53-serine 15 phosphorylation in stimulating transactivation at p53-responsive promoters. *Nucleic Acids Res* **42**, 7666–7680 (2014).
34. Daughtry, B. L. *et al.* Single-cell sequencing of primate preimplantation embryos reveals chromosome elimination via cellular fragmentation and blastomere exclusion. *Genome Res* **29**, 367–382 (2019).
35. Palmerola, K. L. *et al.* Replication stress impairs chromosome segregation and preimplantation development in human embryos. *Cell* (2022) doi:10.1016/j.cell.2022.06.028.

36. Lin, T. *et al.* p53 induces differentiation of mouse embryonic stem cells by suppressing Nanog expression. *Nat Cell Biol* **7**, 165–171 (2005).
37. Vera-Rodriguez, M., Chavez, S. L., Rubio, C., Pera, R. A. R. & Simon, C. Prediction model for aneuploidy in early human embryo development revealed by single-cell analysis. *Nat Commun* **6**, 7601 (2015).
38. Licciardi, F. *et al.* Human blastocysts of normal and abnormal karyotypes display distinct transcriptome profiles. *Sci Rep* **8**, 1–9 (2018).
39. Sanchez-Ribas, I. *et al.* Transcriptomic behavior of genes associated with chromosome 21 aneuploidies in early embryo development. *Fertil Steril* **111**, 991-1001.e2 (2019).
40. Deglincerti, A. *et al.* Self-organization of the in vitro attached human embryo. *Nature* **533**, 251–254 (2016).
41. Shahbazi, M. N. *et al.* Self-organization of the human embryo in the absence of maternal tissues. *Nat Cell Biol* **18**, 700–708 (2016).
42. Kagawa, H. *et al.* Human blastoids model blastocyst development and implantation. *Nature* 1–9 (2021) doi:10.1038/s41586-021-04267-8.
43. Van Landuyt, L. *et al.* Outcome of closed blastocyst vitrification in relation to blastocyst quality: Evaluation of 759 warming cycles in a single-embryo transfer policy. *Human Reproduction* **26**, 527–534 (2011).
44. Love, M. I., Huber, W. & Anders, S. Moderated estimation of fold change and dispersion for RNA-seq data with DESeq2. *Genome Biol* **15**, (2014).
45. Dobin, A. *et al.* STAR: ultrafast universal RNA-seq aligner. *Bioinformatics* **29**, 15–21 (2013).
46. Li, B. & Dewey, C. N. RSEM: accurate transcript quantification from RNA-Seq data with or without a reference genome. *BMC Bioinformatics* **12**, 323 (2011).
47. Robinson, M. D., McCarthy, D. J. & Smyth, G. K. edgeR: A Bioconductor package for differential expression analysis of digital gene expression data. *Bioinformatics* **26**, 139–140 (2009).
48. Ritchie, M. E. *et al.* Limma powers differential expression analyses for RNA-sequencing and microarray studies. *Nucleic Acids Res* **43**, e47 (2015).
49. Robinson, M. D. & Oshlack, A. *A scaling normalization method for differential expression analysis of RNA-seq data*.

http://genomebiology.com/2010/11/3/R25 (2010) doi:10.1186/gb-2010-11-3-r25.

Data availability

Data are available from the corresponding author upon reasonable request.

Acknowledgements

The authors would like to thank Marleen Carlé from the Center for Medical Genetics (UZ Brussel) for assisting during the tubing of trophectoderm samples. We thank Wilfried Cools from the Biostatistics and Medical Informatics Group (VUB) for the statistical advice and the members of the BRIGHTcore facility (UZ Brussel) for performing the RNA sequencing. This study was funded by the Fonds for Scientific Research in Flanders -G017218N- (Fonds Wetenschappelijk Onderzoek – Vlaanderen [FWO]). M.R. and E.C.D.D. are doctoral fellows at the FWO. **Author contributions**

M.R. carried out all the experiments unless stated otherwise, interpreted and analyzed the results and co-wrote the manuscript. Y.L and E.C.D.D. did the bioinformatics analysis. Y.G. performed the trophectoderm biopsies. P.V. provided and supervised the diagnoses of the PGT embryos. G.V. and H.V.D.V. provided the embryos for this study. K.S. interpreted and supervised the experimental work and co-wrote the manuscript. C.S. designed, interpreted and supervised the experimental work and co-wrote the manuscript. All co-authors proofread the manuscript.

Competing interests

The authors declare no competing interests.

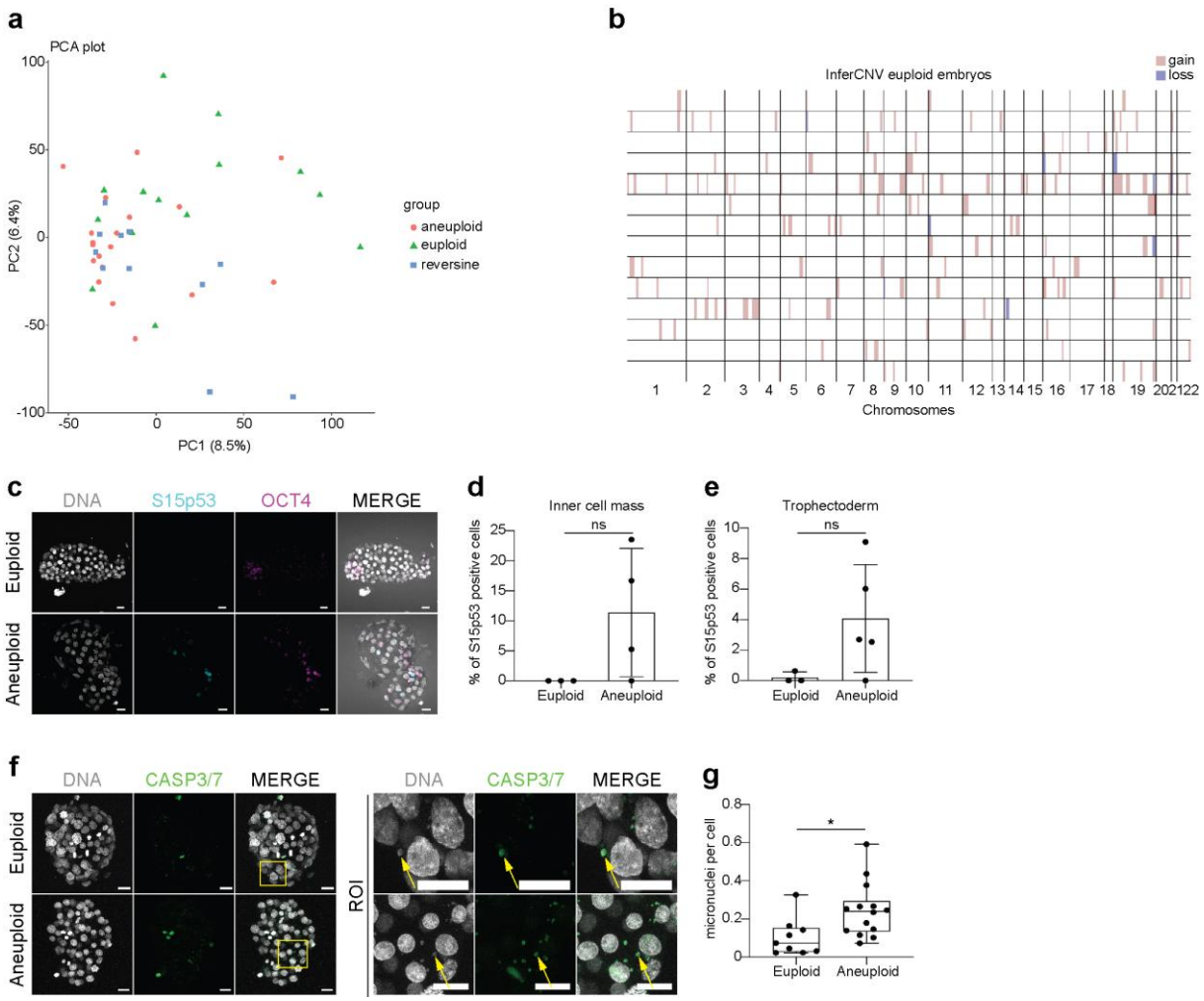

Supplementary Fig. 1:
a, Principal component analysis after RNA-sequencing of euploid (green) versus aneuploid (red) and reversine (blue) embryos. **b**, InferCNV analysis of individual euploid samples compared to the reference set. **c**, Orthogonal projections after immunostaining of euploid and aneuploid embryos for DNA (white), S15p53 (turquoise) and OCT4 (magenta). **d**, Percentages of nuclei positive for S15p53 per embryo in euploid (n = 3) and aneuploid (n = 4) embryos in the ICM. **e**, Percentages of nuclei positive for S15p53 per embryo in euploid (n = 3) and aneuploid (n = 5) embryos in the TE. **f**, Left panel: Orthogonal projections after immunostaining of euploid and aneuploid embryos for DNA (white) and CASP3/7 (green) showing micronuclei. Yellow box indicates zoomed-in region in the right panel. Yellow arrows indicate presence of micronuclei and overlap between DNA and CASP3/7. **g**, Number of micronuclei per cell in euploid and aneuploid whole embryos. Euploid n = 9, Aneuploid n = 14. Student's t-test with Welch's correction, *p = 0.0115.
Brightfield pictures were obtained during confocal imaging. All scale bars are 20 µm. Box and plots show median and minimum to maximum values. Bar plots show mean ± s.d. For all plots each dot represents a single embryo; ns = not significant.